Seasonal variations of mass absorption efficiency of elemental carbon in $PM_{2.5}$ in urban Guangzhou of south China

Chenglei Pei[1,2,3,4], Yunfei Wu[5,*], Jun Tao[6,*], Leiming Zhang[7], Tao Zhang[1,2,3,8], Runqi Zhang[1,2,3], Sheng Li[1,2,3]

[1]State Key Laboratory of Organic Geochemistry and Guangdong Key Laboratory of Environmental Protection and Resources Utilization, Guangzhou Institute of Geochemistry, Chinese Academy of Sciences, Guangzhou, China

[2]CAS Center for Excellence in Deep Earth Science, Guangzhou, China

[3]University of Chinese Academy of Sciences, Beijing, China

[4]Guangzhou Sub-branch of Guangdong Ecological and Environmental Monitoring Center, Guangzhou, China

[5]Key Laboratory of Middle Atmosphere and Global Environment Observation, Institute of Atmospheric Physics, Chinese Academy of Sciences, Beijing, China

[6]Institute for Environmental and Climate Research, Jinan University, Guangzhou, China

[7]Air Quality Research Division, Science and Technology Branch, Environment and Climate Change Canada, Toronto, Canada

[8]GuangDong Ecological and Environmental Monitoring Center, Guangzhou, China

*Correspondence author: (Yunfei Wu) wuyf@mail.iap.ac.cn; (Jun Tao) taojun@jnu.edu.cn

Highlights:

- Vehicle exhaust is the dominant source for carbonaceous aerosols.
- Enhancement of MAE_{EC} compared to "pure EC" was least in summer due to a low degree of EC coating.
- High mass fraction of non-carbonaceous and high RH caused high MAE_{EC}.

Abstract

This study investigates seasonal variations of mass absorption efficiency of elemental carbon (MAE_{EC}) and possible influencing factors in urban Guangzhou of south China. Mass concentrations of elemental carbon (EC) and organic carbon (OC) in $PM_{2.5}$ and aerosol absorption coefficient (b_{ap}) at multi-wavelengths were simultaneously measured in four seasons of 2018–2019 at hourly resolution. Seasonal average mass concentrations of EC were in the range of 1.36–1.70 μgC m^{-3} with a lower value in summer than in the other seasons, while those of OC were in the range of 4.70–6.49 μgC m^{-3} with the lowest value in summer and the highest in autumn. Vehicle exhaust from local traffic was identified to be the predominant source of carbonaceous aerosols. The average aerosol absorption Ångström exponents (AAE) were lower than 1.2 in four seasons, indicating EC and b_{ap} were closely related with vehicle exhaust. Seasonal MAE_{EC} at 550 nm was 11.0, 8.5, 10.4 and 11.3 m^2 g^{-1}, respectively, in spring, summer, autumn, and winter. High MAE_{EC} was related with the high mass ratio of non-carbonaceous aerosols to EC and high ambient relative humidity (RH).

Keywords: vehicle exhaust; non-carbonaceous aerosols; absorption enhancement; relative humidity

1. Introduction

Elemental carbon (EC), also termed as black carbon (BC) from an optical perspective, is the most crucial light absorption matter in atmospheric aerosols (Andreae and Gelencsér, 2006). EC poses direct warming effect, second only to that of CO_2 (Bond et al., 2013). EC also affects visibility and atmospheric stability due to its strong absorption of solar radiation (Ding et al., 2016; Watson, 2002). Thus, knowledge of the optical properties of EC at high temporal resolution in different environments is needed to address air quality and climate issues. One of the key optical properties of EC is its mass absorption efficiency (MAE_{EC}), which is an essential parameter for estimating the contribution of EC to light absorption coefficient (b_{ap}) of atmospheric aerosols. A constant MAE_{EC} value of 6.5 m^2 g^{-1} at 550nm was recommended by the US IMPROVE (Interagency Monitoring of Protected Visual Environments) observation network (Tao et al., 2020). In fact, a wide range of MAE_{EC} values has been reported due to different mixing states of EC with coating aerosols (Cappa et al., 2012; Lack and Cappa, 2010; Peng et al., 2016; Wu et al., 2016b; Zhang et al., 2018). Theoretically, MAE_{EC} would be enhanced by a factor of 2.0 when an EC particle is fully coated by non-absorbing materials with a shell to core diameter ratio as large as 2.8 (Zhang et al., 2017). The dependence of bulk MAE_{EC} in fine particle ($PM_{2.5}$) on the mass ratio of non-absorbing materials to EC is weaker in cleaner than polluted environment where EC emissions are dominated by vehicle exhaust (Cappa et al., 2012; Cappa et al., 2019; Lan et al., 2013), mainly because only a small fraction of EC was well coated by non-

absorbing materials in real world. Size distribution of EC is another important factor influencing MAE_{EC}, e.g., MAE_{EC} could decrease by approximately 6% if the mass median diameter of EC increased from 140 nm to 200 nm (Zhang et al., 2018).

Benefited from a series of emission control measures across China, annual mass concentrations of $PM_{2.5}$ in the Pearl River Delta (PRD) region in south China have decreased evidently since a decade ago and met the national air quality standard (< 35 μg m^{-3}) for many years. However, mass concentrations of EC in $PM_{2.5}$ have not evidently decreased compared to the case of secondary inorganic aerosols (SIAs, e.g., sulfate and nitrate) and organic carbon (OC) due to the large number of vehicle population in urban areas in this region (Tao et al., 2017a). Recently, continuous decreases in OC and sulfate concentrations while an elevation of nitrate concentration and its fraction in $PM_{2.5}$ were observed in urban Guangzhou, a megacity of the PRD region (Li et al., 2021). The change of chemical compositions has already affected the physical and optical properties of $PM_{2.5}$ in this region, e.g., increased the hygroscopicity (Xu et al., 2020; Li et al., 2021). Different change patterns of SIA species and OC, despite the flat EC mass concentration in recent years, certainly would affect MAE_{EC} in this region. However, previous studies mainly focused on the impact of atmospheric aging process and deliquescence of aerosol under the high ambient RH on MAE_{EC} in this region (Sun et al., 2020; Tao et al., 2021). The impact of changes of non-absorbing materials (SIAs and OC) relative to EC on MAE_{EC} has yet to be validated in this region.

To shade some light on the causes of seasonal variations in MAE_{EC}, a measurement

campaign was conducted in an urban environment in Guangzhou in April, July and October of 2018 and January of 2019, which represent four different seasons. During the campaign, hourly mass concentrations of organic carbon (OC), EC, b_{ap}, criteria air pollutants and meteorological parameters were collected. In the following sections, mass concentrations and potential sources of carbonaceous aerosols were first characterized (Section 3.1), aerosol absorption coefficient and its wavelength dependence were then analyzed (Section 3.2), and finally seasonal variations in MAE_{EC} and associated influencing factors were explored (Section 3.3). Knowledge gained from this study is useful in evaluating visibility degradation and regional climate change in South China.

2. Methodology

2.1. Sampling site

The measurement campaign was conducted at a national air quality monitoring site located on the roof of a seven-story building inside the original Guangzhou Environmental Monitoring Center (GEMC) (23.13°N, 113.26°E) in Guangzhou (Fig. 1). There are no obviously industrial emissions within 10 km surrounding the site, but the site is affected by local sources such as traffic and residential activities. The site can be considered to represent typical urban environment in this city. Mass concentrations of EC (C_{EC}) and OC (C_{OC}) and b_{ap} were measured in April, July and October 2018 and January 2019, representing spring, summer, autumn and winter, respectively.

2.2. Online measurement of EC and OC mass concentrations

A model RT-4 Sunset semi-continuous carbon analyzer (Sunset Laboratory Inc, OR, USA) was utilized to measure C_{EC} and C_{OC} with a time resolution of 1 hour. Ambient air, after passing a $PM_{2.5}$ cutoff inlet, was drawn into the carbon analyzer via a 2 m stainless steel tube by the internal pump at a flow rate of 8 L min^{-1}. A denude was installed in front of the carbon analyzer to trap volatile OC. Fine particles were retained on a quartz filter in the first 45 min of each hour, and then delivered into a quartz furnace for OC and EC analysis in the next 15 min using the thermo-optical approach. OC was first vaporized by stepwise heating in a pure helium (He) environment. Subsequently, oxygen was mixed (2 % O_2 in He) to oxidize EC on the filter. The decomposition products of the above two steps were detected by a flame ionization detector to quantify the carbon amounts. During the analysis, a laser beam continuously irradiated the quartz filter. When OC was carbonized with the elevated temperature under the pure He environment, the intensity of transmitted light of the laser gradually decreased. Subsequently, the transmitted light progressively increased with the oxidation and decomposition of carbonized OC and EC under the He/O_2 environment. The moment when the transmitted light was back to its initial intensity was defined as the split point to discriminate OC and EC. The carbon amounts detected before this split point was defined as OC, and that detected afterwards was defined as EC. Operation principle of the carbon analyzer was described in detail by (Birch and Cary, 1996).

2.3. Online measurement of the aerosol absorption coefficient

A model AE-31 aethalometer (Magee Scientific, CA, USA) was used to obtain b_{ap}

at seven wavelengths of 370, 470, 520, 590, 660, 880 and 950 nm with a time resolution of 5 min. The aethalometer was also equipped with a $PM_{2.5}$ cutoff inlet to ensure only fine particles were measured. Meanwhile, a heating device was installed in front of the aethalometer to dry the sample. The value of b_{ap} can be obtained from the measured attenuation (ATN) together with equations (1), (2) and (3), as described in Weingartner et al. (2003):

$$b_{ap} = \frac{ATN}{t} \cdot \frac{A}{Q} \cdot \frac{1}{R(ATN) \cdot C} \quad (1)$$

$$R = \left(\frac{1}{f} - 1\right) \cdot \frac{ln(ATN) - ln(10)}{ln(50) - ln(10)} + 1 \quad (2)$$

$$f = \alpha(1 - \omega) + 1 \quad (3)$$

where t is the sampling time for a single measurement, A is the sampling area on the filter membrane, and Q is the sampling flow rate which was set as 5 L min^{-1} in this study. C and R in Eq. (1) are the two factors introduced to correct the inherent errors in b_{ap} determination using the AE-31 aethalometer. Factor C is used to correct the scattering effect of filter membrane and laden particles which was set as a constant of 3.5 as recommended by WMO (2016). This value is also close to that derived by comparing AE-31 measured attenuation coefficient with the reference b_{ap} obtained by a multi-angle absorption photometer (MAAP) (Wu et al., 2021). Factor R as a function of ATN is employed to correct the loading effect (Weingartner et al., 2003). The variable ω in Eq. (3) represents the single scattering albedo which was set as a mean value of 0.83 in Guangzhou (Andreae et al., 2008), and α is a constant scale factor which was set as 0.86 in this study (Weingartner et al., 2003).

b_{ap} generally exhibits as a power-law function of wavelength (λ), the exponent of which is defined as absorption Ångström exponent (AAE):

$$b_{ap,\lambda} \propto \lambda^{-AAE} \quad (4)$$

In this study, the AAE value is derived from the linear regression of the obtained b_{ap} against the seven wavelengths in the range of 370–950 nm on a logarithm scale, thereby denoted as $AAE_{370\text{-}950nm}$.

2.4. Auxiliary measurements for air pollution and meteorological parameters

Mass concentrations of $PM_{2.5}$ and mixing ratios of gaseous pollutants including SO_2, NO_2, NO, CO and O_3 were obtained from a co-located national air quality station. An automatic weather station (Vaisala Co., Ltd.， Finland) was deployed to provide meteorological data including wind speed, wind direction, temperature, relative humidity (RH) and air pressure.

3. Results and Discussion

3.1. Mass concentrations and potential sources of carbonaceous aerosols

Seasonal average C_{EC} was 1.64 ± 0.84, 1.36 ± 0.57, 1.68 ± 0.81 and 1.70 ± 1.20 μgC m^{-3}, and that of C_{OC} was 5.17 ± 2.29, 4.70 ± 2.35, 6.49 ± 2.43 and 6.09 ± 2.64 μgC m^{-3} in spring, summer, autumn and winter, respectively. Seasonal differences in C_{EC} were very small among spring, autumn and winter, mainly due to the relatively stable primary emissions of EC (e.g., vehicle exhaust) in these seasons in urban Guangzhou (Tao et al., 2017b). The 20% lower C_{EC} in summer than in the other seasons were mainly due to the stronger diffusion (e.g., higher mixing height) and more precipitation

144 scavenging in this season (Fig. 2). Due to the same reason, the lowest seasonal value of
145 C_{OC} also appeared in summer. The highest seasonal average of C_{OC} in autumn might be
146 related with, besides primary fossil combustion, the formation of secondary organic
147 carbon due to the strong photochemical reaction in this season in Guangzhou. Seasonal
148 variations in C_{OC} were also slightly larger than those in C_{EC} due to more factors
149 affecting C_{OC}. In contrast, the highest mass concentration of $PM_{2.5}$ was observed in
150 winter (53.52 ± 22.89 μg m^{-3}), which was 1.9 times higher than that (18.45 ± 5.48 μg
151 m^{-3}) in summer. The much larger seasonal variations in $PM_{2.5}$ than EC and OC
152 suggested the dominant contributions of secondary inorganic aerosols over
153 carbonaceous aerosols to $PM_{2.5}$ in this city.

154 Moderate correlations ($R^2 \geq 0.58$, $p < 0.01$) between hourly C_{OC} and C_{EC} were
155 found in all the seasons (Fig. 3), with the slopes of 2.3, 3.1, 2.7 and 1.9, in spring,
156 summer, autumn and winter, respectively, implying the homogenic sources of
157 carbonaceous aerosols in urban Guangzhou (Tao et al., 2017b). The relatively high
158 slopes (OC/EC ratios) in the present study than reported previously for this city (Tao et
159 al., 2014; Tao et al., 2017b) were likely due to the different method protocols (e.g.,
160 NIOSH-TOT protocol and IMPROVE-TOR protocol) (Cheng et al., 2011; Wu et al.,
161 2016a). On average, the determined C_{EC} by IMPROVE-TOR protocol (denoted as $C_{EC\text{-}TOR}$)
162 was 2.2 times of that by NIOSH-TOT protocol (denoted as $C_{EC\text{-}TOT}$) in urban areas
163 in the PRD region (Wu et al., 2016a). Taking into account this conversion factor, the
164 seasonal slopes between C_{OC} and C_{EC} under the IMPROVE-TOR protocol in this study

(Fig. S1) are comparable to those (0.77–1.52) directly determined using IMPROVE-TOR protocol in previous studies (Tao et al., 2017b; Tao et al., 2014). The estimated OC/EC ratios under IMPROVE-TOR protocol are close to that of vehicle exhaust (1.1) and generally lower than those of coal combustion (2.7) and biomass burning (9.0) (Watson et al., 2001). These values implied the predominant contribution of traffic emissions to carbonaceous aerosols in urban Guangzhou.

In addition, moderate correlations ($R^2 \geq 0.55$, $p < 0.01$) between hourly C_{EC} and NO_x ($NO+NO_2$) mixing ratio were found in all the seasons except summer (Fig. 4), further indicating the predominant contribution of traffic emissions to EC (Bos et al., 2021). The poor correlation in summer was likely due to frequent rainfall, which removed particles more effectively than did insoluble gases (such as NO_x). Similarly, OC was also very likely mainly from vehicle exhaust emissions followed by secondary aerosol formation in this city.

3.2. Aerosol absorption coefficient and its wavelength dependence

b_{ap} at 950nm ($b_{ap,950nm}$) showed a similar seasonal pattern to that of C_{EC} due to the predominant contribution of EC to aerosol light absorption at infrared wavelengths. The highest seasonal average of $b_{ap,950nm}$ was found in winter (10.43 ± 7.09 Mm^{-1}), which was 1.6 times of the lowest one in summer (6.50 ± 2.65 Mm^{-1}). Note that the average C_{EC} in winter is only 1.2 times of that in summer. The slightly different scales of seasonal variations between $b_{ap,950nm}$ and C_{EC} suggested other factors besides EC mass might also affect $b_{ap,950nm}$, e.g., coating fraction and coating thickness (Lack and Cappa,

2010; Lan et al., 2013; Zhang et al., 2018).

Wavelength dependence of b_{ap} could also be used to investigate the sources of carbonaceous aerosols. Generally, AAE in urban areas dominated by traffic emissions has a value of approximately 1.0, and a value larger than 1.6 when dominated by biomass burning (Blanco-Alegre et al., 2020; Lack and Cappa, 2010). As shown in Fig. 2b, hourly AAE varied in a range of 0.82–1.60 during the whole measurement period, indicating negligible contributions from biomass burning to b_{ap}.

Seasonal $AAE_{370\text{-}950nm}$ calculated using Eq. 4 was 1.07, 1.09, 1.19 and 1.17in spring, summer, autumn and winter, respectively, in urban Guangzhou (Fig. 5). $AAE_{370\text{-}950nm}$ values in all the seasons were evidently lower than those from biomass burning, suggesting negligible contributions of brown carbon (BrC) from biomass and/or biofuel burning to $AAE_{370\text{-}950nm}$ in urban Guangzhou. The slightly larger $AAE_{370\text{-}950nm}$ in autumn and winter than in spring and summer was likely due to the seasonal differences in EC morphology, size distribution and mixing state (Gyawali et al., 2012; Zhang et al., 2020). The values of $AAE_{370\text{-}950nm}$ in the present study were consistent with previous results obtained in urban Guangzhou in 2015–2016 (Tao et al., 2021) and other cities in the PRD region, e.g., 1.1 in urban Shenzhen (Lan et al., 2013; Li et al., 2018) and 1.0–1.1 in Hong Kong (Lan et al., 2013; Li et al., 2018). These results further supported that EC was mainly emitted from vehicle emissions in the urban areas of the PRD region.

3.3. Seasonal variations in MAE_{EC} and influencing factors

Good correlations ($R^2 \geq 0.85$, $p < 0.01$)) between b_{ap} and C_{EC} were found in four

seasons (Fig. 6), indicating the dominant impact of EC mass on b_{ap} at infrared wavelengths. Considering the negligible contribution of BrC to b_{ap} at infrared wavelengths, the slope of zero-intercept linear regression of b_{ap} against C_{EC} can be considered as the bulk MAE_{EC} at 950 nm ($MAE_{EC,950nm}$). The derived bulk $MAE_{EC,950nm}$ showed pronounced seasonal variations, with values of 6.13, 4.69, 5.44 and 5.97 $m^2\ g^{-1}$ in spring, summer, autumn and winter, respectively, indicating seasonal variations in microphysical properties (e.g., mixing state, size distribution) of EC.

Bulk MAE_{EC} at 550 nm ($MAE_{EC,550nm}$), an intermediate wavelength in solar spectrum commonly concerned by previous studies (Bond and Bergstrom, 2006), can be estimated from $MAE_{EC,950nm}$ and seasonal AAE using Eq. (4). The derived $MAE_{EC,550nm}$ are 11.00, 8.51, 10.42 and 11.32 $m^2\ g^{-1}$ in spring, summer, autumn and winter, respectively. Compared to "pure EC" with a mean $MAE_{EC,550nm}$ of 7.5 $m^2\ g^{-1}$, seasonal $MAE_{EC,550nm}$ were enhanced by 47%, 13%, 39% and 51% in spring, summer autumn and winter, respectively (Bond and Bergstrom, 2006). The lowest enhancement in summer was likely due to a low degree of coating of EC in this season. Low amplifications of MAE in summer (or wet season) were also found in previous studies in urban areas of the PRD region (Lan et al., 2013; Sun et al., 2020).

The amplifications of MAE_{EC} observed in the present study were comparable to those previously obtained in other urban regions worldwide (Andreae et al., 2008; Favez et al., 2009; Kondo et al., 2009; Lan et al., 2013; Liu et al., 2019; Ma et al., 2020; Sun et al., 2020; Wang et al., 2014; Wu et al., 2016b). Ma et al. (2020) observed a

slightly wavelength-dependent absorption enhancement of 1.35–1.42 in Nanjing of the Yangtze River Delta region, which was attributed to the coating of particulate nitrate on BC particles from traffic emissions. Liu et al. (2019) found 1.4- and 1.6-times enhancements of BC absorption (870 nm) for summer and winter respectively in urban Beijing of the North China Plain region when $PM_1 > 50$ μg m^{-3}. Wang et al. (2014) obtained an average enhancement of 1.8 for BC absorption at 870 nm in a severely polluted urban region (Xi'an) of Northwest China. Generally, polluted environments combined with humid conditions are conducive to EC absorption enhancement by providing abundant secondary components for coating aged EC particles (Ma et al., 2020; Wu et al., 2016b). The amplifications of MAE_{EC} in this study were also comparable to those obtained in urban Guangzhou in previous years of 2017–2018 presented by Sun et al. (2020), although a different approach named minimum R squared method was used to determine absorption enhancement in their study. However, increases in the MAE_{EC} enhancements were observed when compared to those obtained in all the seasons of 2015–2016 expect summer, likely related to the increasing nitrate fraction in $PM_{2.5}$ (Li et al., 2021). Increasing nitrate not only provided abundant materials for EC coatings but also increased aerosol hygroscopicity (Xu et al., 2020), which is further conductive to the internal mixing of EC with water-soluble matters (Tao et al., 2021).

Regarding diurnal pattern of MAE_{EC} in urban areas of the PRD region, a clear afternoon peak was previously observed, corresponding well to the peak of number

fraction of core-shell mixed rBC particles out of total rBC-containing particles (an indicator of rBC coating degree) and the peak of O_3 mixing ratio (Lan et al., 2013). Thus, MAE_{EC} was considered to be largely affected by photochemical processes. However, in the present study, no evident diurnal variations of MAE_{EC} were found in any of the four seasons in urban Guangzhou, despite apparent afternoon peaks of OC/EC ratio and O_3 concentration (Fig. 7). Note that hourly MAE_{EC} investigated in the diurnal variations was calculated by hourly $b_{ap,950nm}$ divided by hourly C_{EC}. In addition, no significant correlation (R^2=0.02) was found between daily $MAE_{EC,950nm}$ and OC/EC ratio, implying limited influence of OC on the mixing state of EC in this city. A large fraction of OC was attributed to secondary OC (SOC) mostly generated from gas-phase reactions rather than heterogeneous reactions in urban Guangzhou (Chen et al., 2021), implying SOC is likely externally mixed with EC, thereby has limited contribution to the absorption enhancement of EC.

By contrast, daily $MAE_{EC,950nm}$ positively correlated with mass fraction of non-carbonaceous aerosol components in $PM_{2.5}$ (R^2=0.50, p<0.01) (Fig. 8a). Note that the mass concentration of non-carbonaceous aerosol components is calculated as the difference between $PM_{2.5}$ and the total of EC and organic matter (1.6×OC) (Zhang et al., 2013). Because the relatively low contributions of mineral aerosols and trace metals to $PM_{2.5}$ in urban Guangzhou (Tao et al., 2014), the non-carbonaceous aerosol components are mostly attributed to secondary inorganic aerosols (SIAs), such as sulfate, nitrate and ammonium. The lowest $MAE_{EC,950nm}$ in summer was likely due to

the lowest mass fraction of non-carbonaceous aerosols in $PM_{2.5}$ (triangles in Fig. 8a). In addition, higher $MAE_{EC,950nm}$ was also closely related with higher RH under the same mass fraction of non-carbonaceous aerosols in $PM_{2.5}$ (Fig. 8a). High RH leads to high water content in aerosols, which is conducive to EC core embedding into water-soluble SIA components. Furthermore, high RH also favors the heterogeneous formation of SIAs on the surface of EC particles, thereby increasing the probability of core-shell mixing (Wu et al., 2016b). Thus, ambient RH also plays a role on the variation of $MAE_{EC,950nm}$, which partly interpreted the relatively lower $MAE_{EC,950nm}$ in autumn (with low RH) than spring and winter, despite higher mass fraction of non-carbonaceous aerosol in autumn.

In addition, daily $MAE_{EC,950nm}$ decreased with increasing mass fraction of EC in $PM_{2.5}$ (Fig. 8b), likely because a low fraction of EC in $PM_{2.5}$ was due to a high coating extent of EC by non-carbonaceous aerosols. Such a hypothesis is supported by the fact that EC was mainly from locally produced vehicle exhaust inside the city while non-carbonaceous aerosols (mainly secondary inorganic aerosols) were mostly from regional transport of industrial emission produced outside the city (Tao et al., 2017b).

4. Conclusions

To investigate the seasonal variations of MAE_{EC} and associated dominant factors, hourly C_{EC}, C_{OC} and b_{ap} of $PM_{2.5}$ were simultaneously measured in urban Guangzhou in four seasons of 2018-2019. Moderate correlations between C_{EC} and C_{OC} were observed with low OC/EC mass ratios. C_{EC} also moderately correlated with NOx

mixing ratio. These facts demonstrated that carbonaceous aerosols were mainly from vehicle emissions in this city. The seasonal average AAE values were generally lower than 1.2 in all the seasons, indicating the dominant contribution of vehicle exhaust to b_{ap} in the spectrum range of 370–950 nm. In this environment dominated by traffic emissions, the estimated bulk $MAE_{EC,550nm}$ was 1.13–1.51 times of the mean value of 7.5 m^2 g^{-1} commonly used for "pure EC", implying the absorption enhancement of EC particles due to coating. The enhanced MAE_{EC} compared to "pure EC" was mainly related with high non-carbonaceous (mostly SIAs) factions in $PM_{2.5}$ rather than photochemically produced SOC, as well high ambient RH. Results revealed the importance of further reducing the SIAs, particularly nitrate, to improve visibility and mitigate warming effects induced by EC absorption in the PRD region. Furthermore, accurately quantifying the value of MAE_{EC} is largely affected by the measurement methods for both C_{EC} and b_{ap}. Thus, in future, measurements based on more advantage methods, e.g., photoacoustic soot spectrometer (PASS) for C_{EC} and single particle soot photometer (SP2) for b_{ap}, are needed and suggested to compare with those used in this study to provide more reliable quantification of MAE_{EC} in this region.

Data availability. Data used in this study are available from Jun Tao (taojun@jnu.edu.cn).

Competing interests. The authors declare that they have no conflict of interest.

Acknowledgments

This study was supported by the National Natural Science Foundation of China (No.

41775155, 41875160 and 41475119).

References

Andreae, M O, Gelencsér, A, 2006. Black carbon or brown carbon? The nature of light-absorbing carbonaceous aerosols. Atmospheric Chemistry Physics 6:3131-3148.

Andreae, M O, Schmid, O, Yang, H, Chand, D, Yu, J Z, Zeng, L-M, Zhang, Y-H, 2008. Optical properties and chemical composition of the atmospheric aerosol in urban Guangzhou, China. Atmospheric Environment 42:6335-6350.

Birch, M E, Cary, R A, 1996. Elemental Carbon-Based Method for Monitoring Occupational Exposures to Particulate Diesel Exhaust. Aerosol Science and Technology 25:221-241.

Blanco-Alegre, C, Calvo, A I, Alves, C, Fialho, P, Nunes, T, Gomes, J, Castro, A, Oduber, F, Coz, E, Fraile, R, 2020. Aethalometer measurements in a road tunnel: A step forward in the characterization of black carbon emissions from traffic. Science of The Total Environment 703:135483.

Bond, T C, Bergstrom, R W, 2006. Light absorption by carbonaceous particles: An investigative review. Aerosol Science and Technology 40:27-67.

Bond, T C, Doherty, S J, Fahey, D W, Forster, P M, Berntsen, T, Deangelo, B, Flanner, M G, Ghan, S J, Karcher, B, Koch, D, 2013. Bounding the role of black carbon in the climate system: A scientific assessment. Journal of Geophysical Research 118:5380-5552.

Bos, B, Lim, S, Hedges, M, Molden, N, Boyle, S, Mudway, D I, Barratt, D B, 2021. Taxi drivers' exposure to black carbon and nitrogen dioxide in electric and diesel vehicles: A case study in London. Environmental Research 195:110736.

Cappa, C D, Onasch, T B, Massoli, P, Worsnop, D R, Bates, T S, Cross, E S, Davidovits, P, Hakala, J, Hayden, K L, Jobson, B T, Kolesar, K R, Lack, D A, Lerner, B M, Li, S-M, Mellon, D, Nuaaman, I, Olfert, J S, Petäjä, T, Quinn, P K, Song, C, Subramanian, R, Williams, E J, Zaveri, R A, 2012. Radiative Absorption Enhancements Due to the Mixing State of Atmospheric Black Carbon. 337:1078-1081.

Cappa, C D, Zhang, X, Russell, L M, Collier, S, Lee, A K Y, Chen, C-L, Betha, R, Chen, S, Liu, J, Price, D J, Sanchez, K J, McMeeking, G R, Williams, L R, Onasch, T B, Worsnop, D R, Abbatt, J, Zhang, Q, 2019. Light Absorption by Ambient Black and Brown Carbon and its Dependence on Black Carbon Coating State for Two California, USA, Cities in Winter and Summer. 124:1550-1577.

Chen, W, Ye, Y Q, Hu, W W, Zhou, H S, Pan, T L, Wang, Y K, Song, W, Song, Q C, Ye, C S, Wang, C M, Wang, B L, Huang, S, Yuan, B, Zhu, M, Lian, X F, Zhang, G H, Bi, X H, Jiang, F, Liu, J M, Canonaco, F, Prevot, A S H, Shao, M, Wang, X M, 2021. Real-time characterization of aerosol compositions, sources, and aging processes in Guangzhou during PRIDE-GBA 2018

campaign. Journal of Geophysical Research: Atmospheres 126: e2021JD035114.

Cheng, Y., Duan, F.-K., He, K.-B., Zheng, M., Du, Z.-Y., Ma, Y.-L., and Tan, J.-H., 2011. Intercomparison of thermal–optical methods for the determination of organic and elemental carbon: influences of aerosol composition and implications. Environ. Sci. Technol. 45: 10117–10123.

Ding, A J, Huang, X, Nie, W, Sun, J N, Kerminen, V-M, Petäjä, T, Su, H, Cheng, Y F, Yang, X-Q, Wang, M H, Chi, X G, Wang, J P, Virkkula, A, Guo, W D, Yuan, J, Wang, S Y, Zhang, R J, Wu, Y F, Song, Y, Zhu, T, Zilitinkevich, S, Kulmala, M, Fu, C B, 2016. Enhanced haze pollution by black carbon in megacities in China. 43:2873-2879.

Favez, O, Alfaro, S C, Sciare, J, Cachier, H, Abdelwahab, M M, 2009. Ambient measurements of light-absorption by agricultural waste burning organic aerosols. Journal of Aerosol Science 40:613-620.

Gyawali, M, Arnott, W P, Zaveri, R A, Song, C, Moosmüller, H, Liu, L, Mishchenko, M I, Chen, L W A, Green, M C, Watson, J G, Chow, J C, 2012. Photoacoustic optical properties at UV, VIS, and near IR wavelengths for laboratory generated and winter time ambient urban aerosols. Atmos. Chem. Phys. 12:2587-2601.

Kondo, Y, Sahu, L, Kuwata, M, Miyazaki, Y, Takegawa, N, Moteki, N, Imaru, J, Han, S, Nakayama, T, Oanh, N K, 2009. Stabilization of the mass absorption cross section of black carbon for filter-based absorption photometry by the use of a heated inlet. Aerosol Science and Technology 43:741-756.

Lack, D A, Cappa, C D, 2010. Impact of brown and clear carbon on light absorption enhancement, single scatter albedo and absorption wavelength dependence of black carbon. Atmos. Chem. Phys. 10:4207-4220.

Lan, Z-J, Huang, X-F, Yu, K-Y, Sun, T-L, Zeng, L-W, Hu, M, 2013. Light absorption of black carbon aerosol and its enhancement by mixing state in an urban atmosphere in South China. Atmospheric Environment 69:118-123.

Li, G-L, Sun, L, Ho, K-F, Wong, K-C, Ning, Z, 2018. Implication of Light Absorption Enhancement and Mixing State of Black Carbon (BC) by Coatings in Hong Kong. Aerosol and Air Quality Research 18:2753-2763.

Li, J. W., Zhang, Z. S., Wu, Y. F., Tao, J., Xia, Y. J., Wang, C. Y., and Zhang, R., 2021. Effects of chemical compositions in fine particles and their identified sources on hygroscopic growth factor during dry season in urban Guangzhou of South China. Science of the Total Environment 801: 149749.

Liu, D, Joshi, R, Wang, J, Yu, C, Allan, J D, Coe, H, Flynn, M J, Xie, C, Lee, J, Squires, F, 2019. Contrasting physical properties of black carbon in urban Beijing between winter and summer. Atmospheric Chemistry Physics:6749-6769.

Ma, Y, Huang, C, Jabbour, H, Zheng, Z, Wang, Y, Jiang, Y, Zhu, W, Ge, X, Collier, S, Zheng, J, 2020. Mixing state and light absorption enhancement of black carbon aerosols in summertime Nanjing, China. Atmospheric Environment 222:117141.

Peng, J, Hu, M, Guo, S, Du, Z, Zheng, J, Shang, D, Levy Zamora, M, Zeng, L, Shao, M, Wu, Y-S, Zheng, J, Wang, Y, Glen, C R, Collins, D R, Molina, M J, Zhang, R, 2016. Markedly enhanced absorption and direct radiative forcing of black carbon under polluted urban environments. 113:4266-4271.

Sun, J Y, Wu, C, Wu, D, Cheng, C, Li, M, Li, L, Deng, T, Yu, J Z, Li, Y J, Zhou, Q, Liang, Y, Sun, T, Song, L, Cheng, P, Yang, W, Pei, C, Chen, Y, Cen, Y, Nian, H, Zhou, Z, 2020. Amplification of black carbon light absorption induced by atmospheric aging: temporal variation at seasonal and diel scales in urban Guangzhou. Atmos. Chem. Phys. 20:2445-2470.

Tao, J, Zhang, L, Cao, J, Zhang, R, 2017a. A review of current knowledge concerning PM2. 5 chemical composition, aerosol optical properties and their relationships across China. Atmospheric Chemistry Physics 17:9485-9518.

Tao, J, Zhang, L, Cao, J, Zhong, L, Chen, D, Yang, Y, Chen, D, Chen, L, Zhang, Z, Wu, Y, Xia, Y, Ye, S, Zhang, R, 2017b. Source apportionment of PM2.5 at urban and suburban areas of the Pearl River Delta region, south China - With emphasis on ship emissions. Science of The Total Environment 574:1559-1570.

Tao, J, Zhang, L, Ho, K, Zhang, R, Lin, Z, Zhang, Z, Lin, M, Cao, J, Liu, S, Wang, G, 2014. Impact of PM2.5 chemical compositions on aerosol light scattering in Guangzhou — the largest megacity in South China. Atmospheric Research 135-136:48-58.

Tao, J, Zhang, L, Wu, Y, Zhang, Z, 2020. Evaluation of the IMPROVE formulas based on Mie model in the calculation of particle scattering coefficient in an urban atmosphere. Atmospheric Environment 222:117116.

Tao, J, Zhang, Z, Zhang, L, Wu, Y, Zhang, R, Wang, B, 2021. Impact of deliquescence of aerosol on mass absorption efficiency of elemental carbon in fine particles in urban Guangzhou in south China. Atmospheric Environment 256:118476.

Wang, Q, Huang, R-J, Cao, J, Han, Y, Wang, G, Li, G, Wang, Y, Dai, W, Zhang, R, Zhou, Y, 2014. Mixing state of black carbon aerosol in a heavily polluted urban area of China: Implications for light absorption enhancement. Aerosol Science and Technology 48:689-697.

Watson, J G, 2002. Visibility: Science and Regulation. Journal of the Air & Waste Management Association 52:628-713.

Watson, J G, Chow, J C, Houck, J E, 2001. PM2.5 chemical source profiles for vehicle exhaust, vegetative burning, geological material, and coal burning in Northwestern Colorado during 1995. Chemosphere 43:1141-1151.

Weingartner, E, Saathoff, H, Schnaiter, M, Streit, N, Bitnar, B, Baltensperger, U, 2003. Absorption of light by soot particles: determination of the absorption coefficient by means of aethalometers.

Journal of Aerosol Science 34:1445-1463.

Wu, C, Huang, X H H, Ng, W M, Griffith, S M, Yu, J Z, 2016a. Inter-comparison of NIOSH and IMPROVE protocols for OC and EC determination: implications for inter-protocol data conversion. Atmos. Meas. Tech. 9:4547-4560.

Wu, Y, Li, J, Jiang, C, Xia, Y, Tao, J, Tian, P, Zhou, C, Wang, C, Xia, X, Huang, R-j, Zhang, R, 2021. Spectral absorption properties of organic carbon aerosol during a polluted winter in Beijing, China. Science of The Total Environment 755:142600.

Wu, Y, Zhang, R, Tian, P, Tao, J, Hsu, S-C, Yan, P, Wang, Q, Cao, J, Zhang, X, Xia, X, 2016b. Effect of ambient humidity on the light absorption amplification of black carbon in Beijing during January 2013. Atmospheric Environment 124:217-223.

Xu, Y. W., Kuang, Y., Bian, Y. X., Liu, L., Li, F., Wang, Y. Q., Xue, B., Luo, B., Huang, S., Yuan, B., Zhao, P. S., and Shao, M., 2020. Current changllenges in visibility improvement in Southern China. Environmental Science & Technology Letters 7(6): 395-401.

Zhang, R, Jing, J, Tao, J, Hsu, S C, Wang, G, Cao, J, Lee, C S L, Zhu, L, Chen, Z, Zhao, Y, Shen, Z, 2013. Chemical characterization and source apportionment of PM2.5 in Beijing: seasonal perspective. Atmos. Chem. Phys. 13:7053-7074.

Zhang, X, Mao, M, Yin, Y, Tang, S, 2020. The absorption Ångstrom exponent of black carbon with brown coatings: effects of aerosol microphysics and parameterization. Atmos. Chem. Phys. 20:9701-9711.

Zhang, X, Mao, M, Yin, Y, Wang, B, 2017. Absorption enhancement of aged black carbon aerosols affected by their microphysics: A numerical investigation. Journal of Quantitative Spectroscopy and Radiative Transfer 202:90-97.

Zhang, Y, Zhang, Q, Cheng, Y, Su, H, Li, H, Li, M, Zhang, X, Ding, A, He, K, 2018. Amplification of light absorption of black carbon associated with air pollution. Atmos. Chem. Phys. 18:9879-9896.

List of Figures

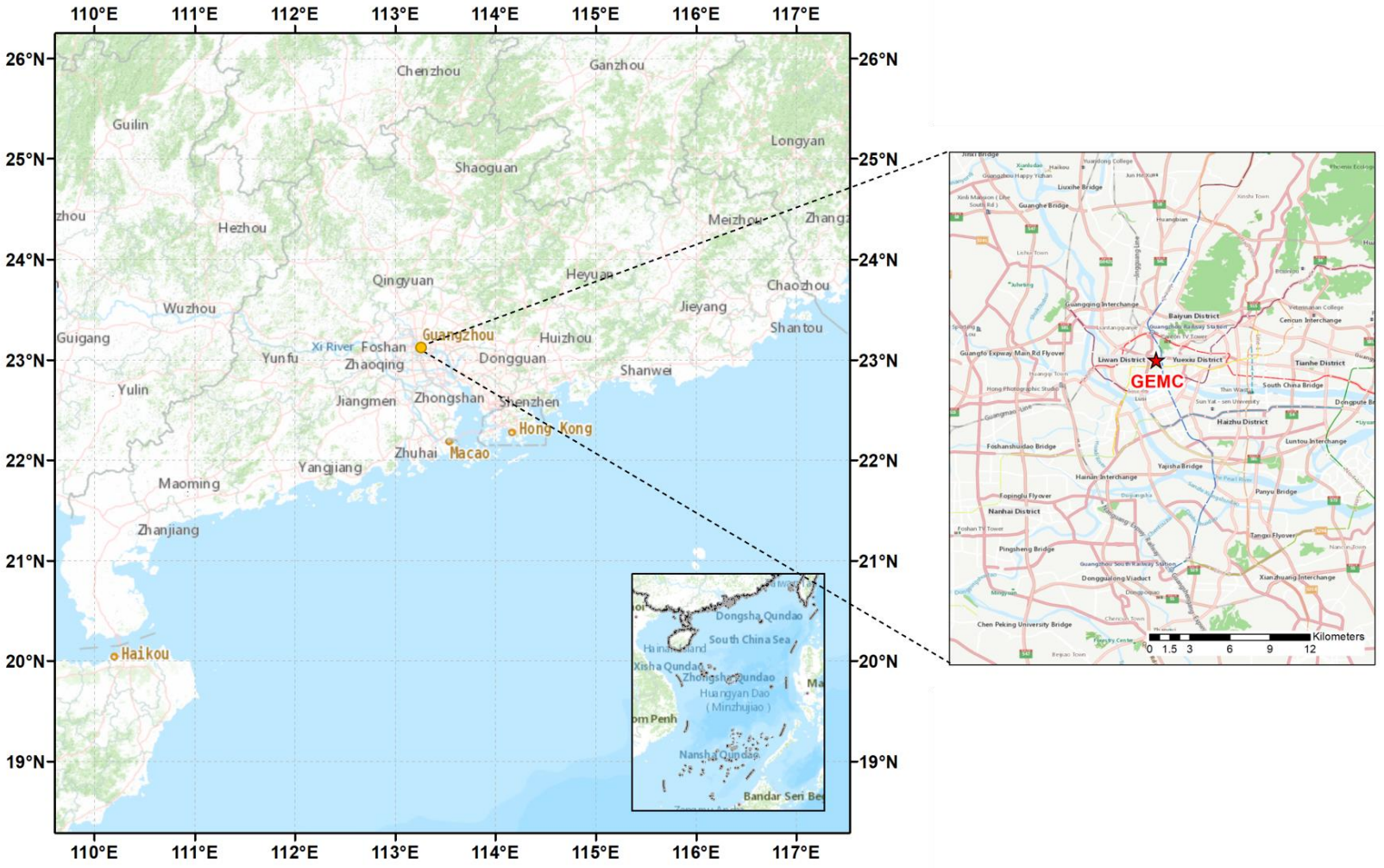
110°E
111°E
112°E
113°E
114°E
115°E
116°E
117°E
26°N
25°N
24°N
23°N
22°N
21°N
20°N
19°N
Chenzhou
Ganzhou
Guilin
Longyan
Shaoguan
Hezhou
Meizhou
Qingyuan
Heyuan
Chaozhou
Wuzhou
Jieyang
Shantou
Guigang
Guangzhou
Huizhou
Xi River
Foshan
Yunfu
Zhaoqing
Dongguan
Shanwei
Yulin
Jiangmen
Zhongshan
Shenzhen
Hong Kong
Zhuhai
Macao
Yangjiang
Maoming
Zhanjiang
Haikou
Dongsha Qundao
South China Sea
Xisha Qundao
Zhongsha Qundao
Huangyan Dao
(Minzhujiao)
Nansha Qundao
Bandar Seri Be
GEMC
Liwan District
Yuexiu District
Baiyun District
Tianhe District
Haizhu District
Nanhai District
Kilometers
0 1.5 3 6 9 12

Fig.1

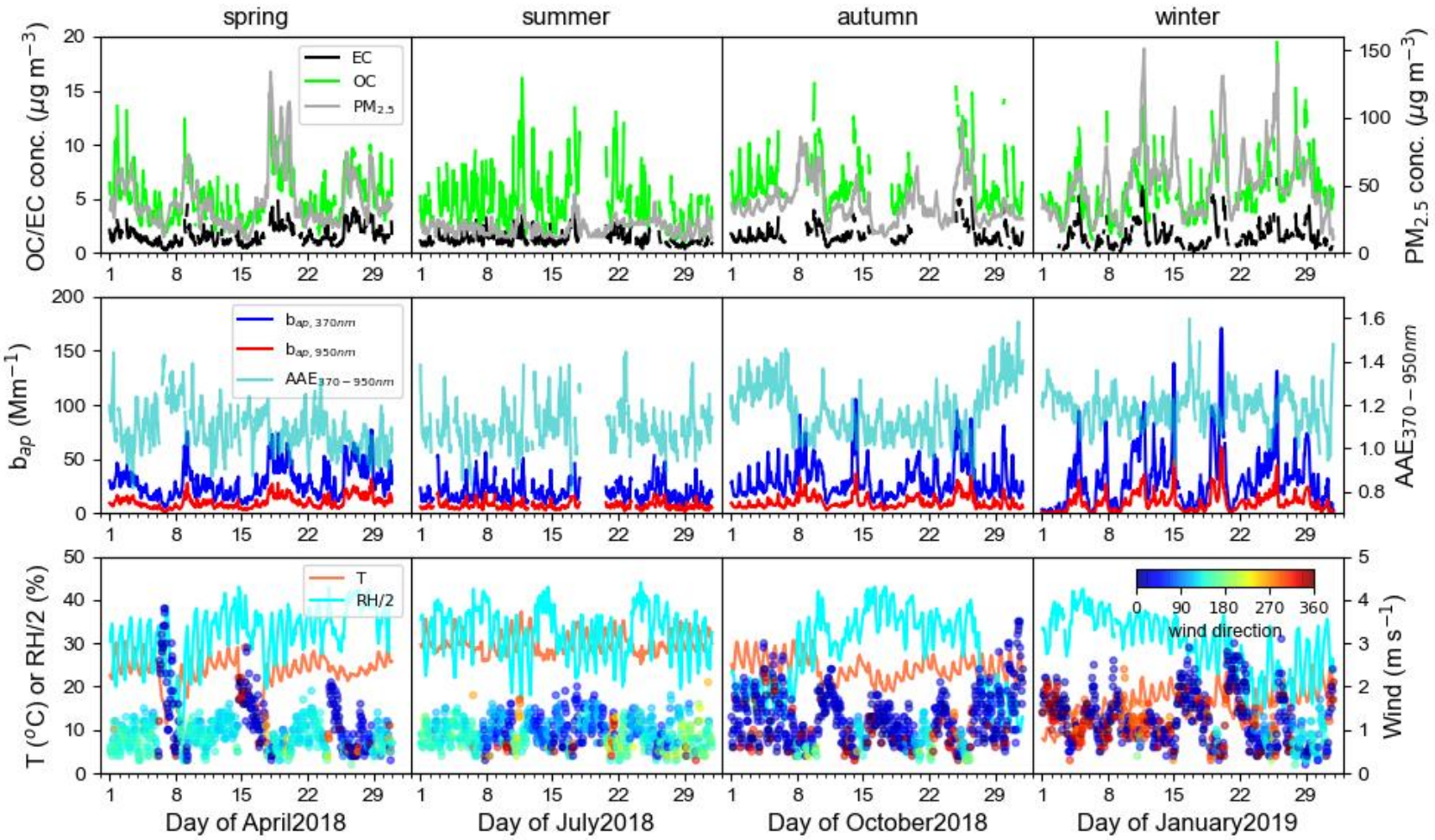
spring
summer
autumn
winter
EC
OC
PM2.5
OC/EC conc. (μg m−3)
PM2.5 conc. (μg m−3)
bap, 370nm
bap, 950nm
AAE370 − 950nm
bap (Mm−1)
T
RH/2
T (°C) or RH/2 (%)
wind direction
Wind (m s−1)
Day of April2018
Day of July2018
Day of October2018
Day of January2019

Fig.2

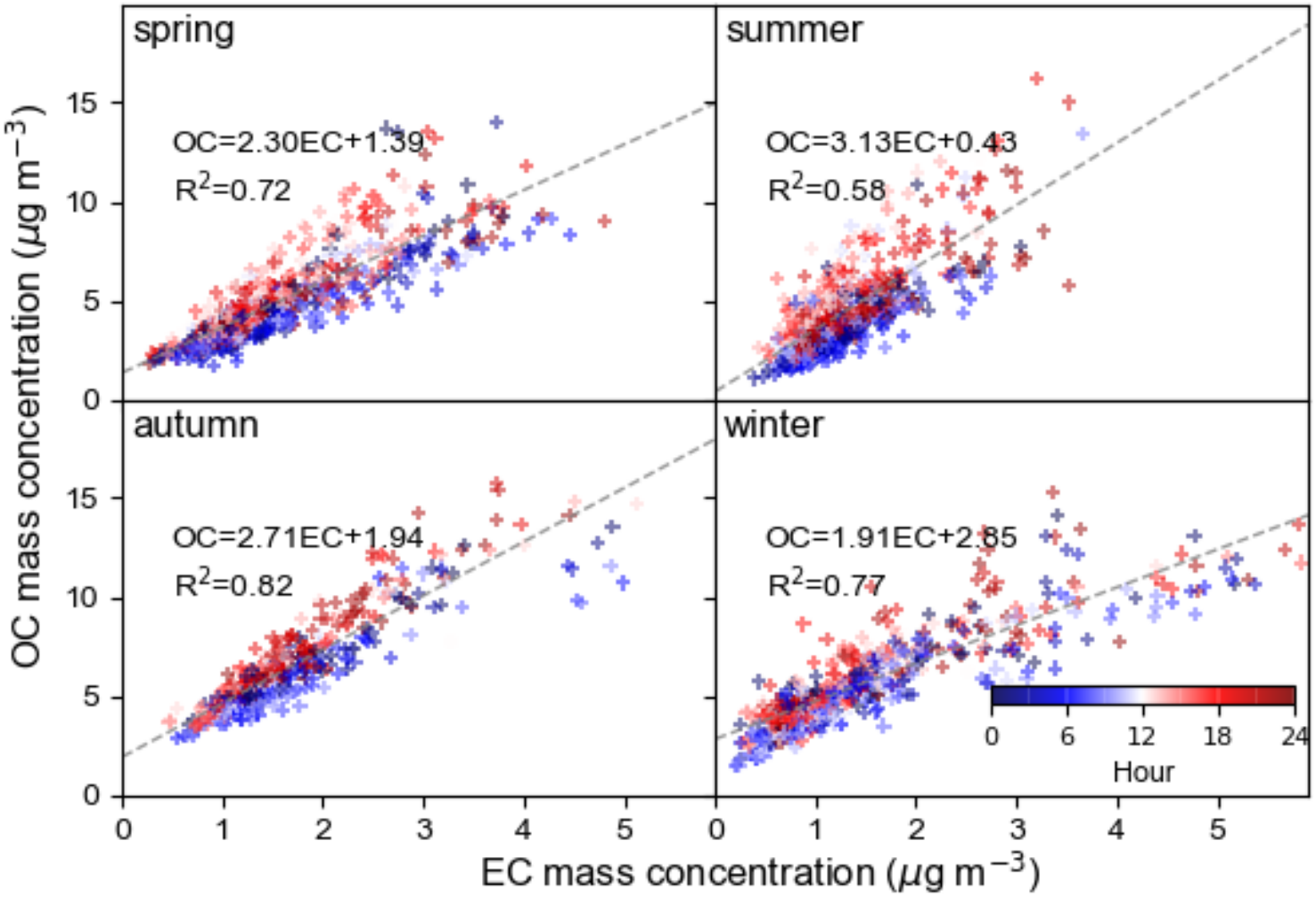
spring
OC=2.30EC+1.39
R2=0.72
summer
OC=3.13EC+0.43
R2=0.58
autumn
OC=2.71EC+1.94
R2=0.82
winter
OC=1.91EC+2.85
R2=0.77
0
6
12
18
24
Hour
OC mass concentration (μg m−3)
EC mass concentration (μg m−3)

Fig.3

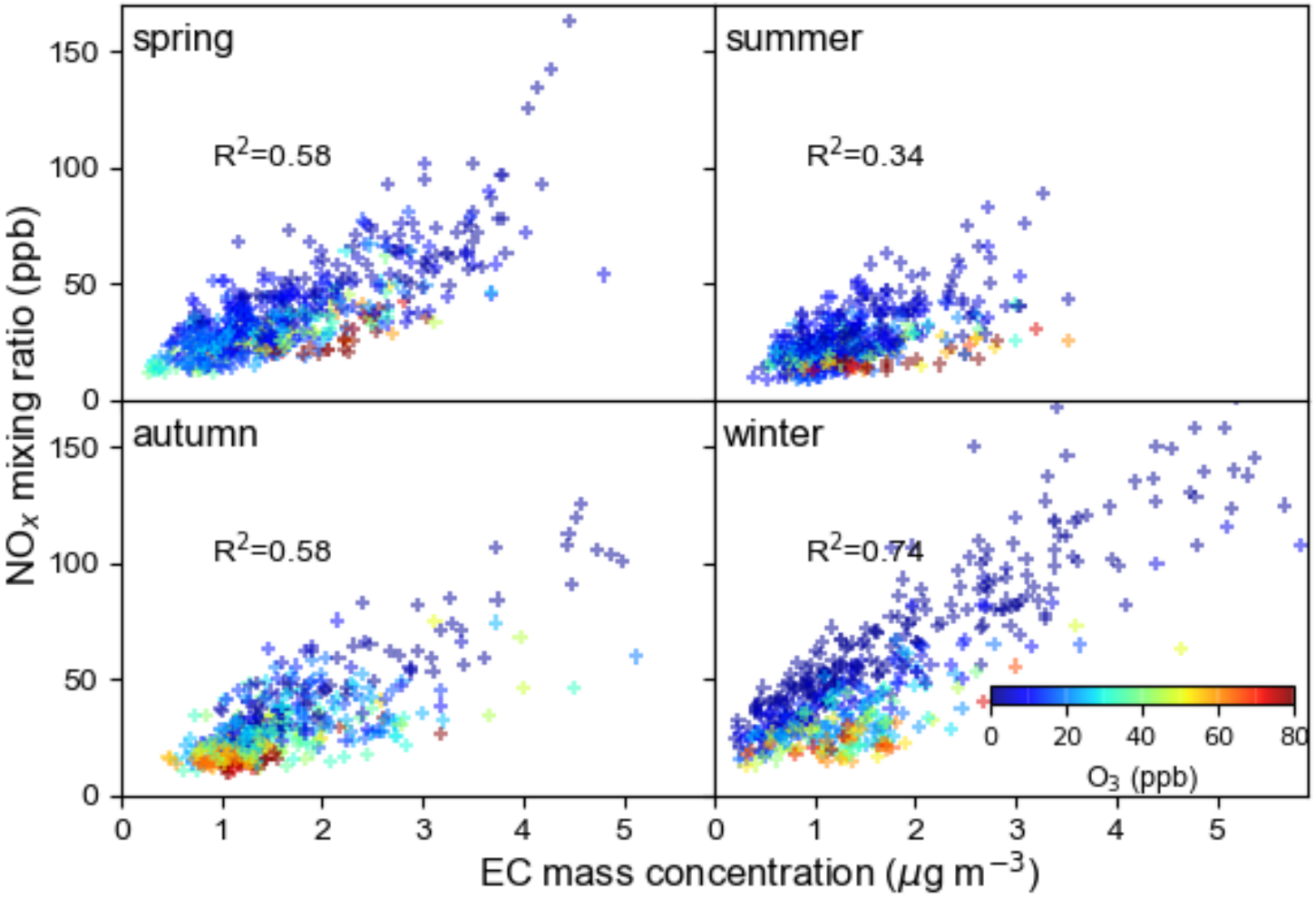
spring
summer
autumn
winter
R2=0.58
R2=0.34
R2=0.58
R2=0.74
NOx mixing ratio (ppb)
EC mass concentration (μg m−3)
O3 (ppb)
0
20
40
60
80
0
50
100
150
1
2
3
4
5

Fig.4

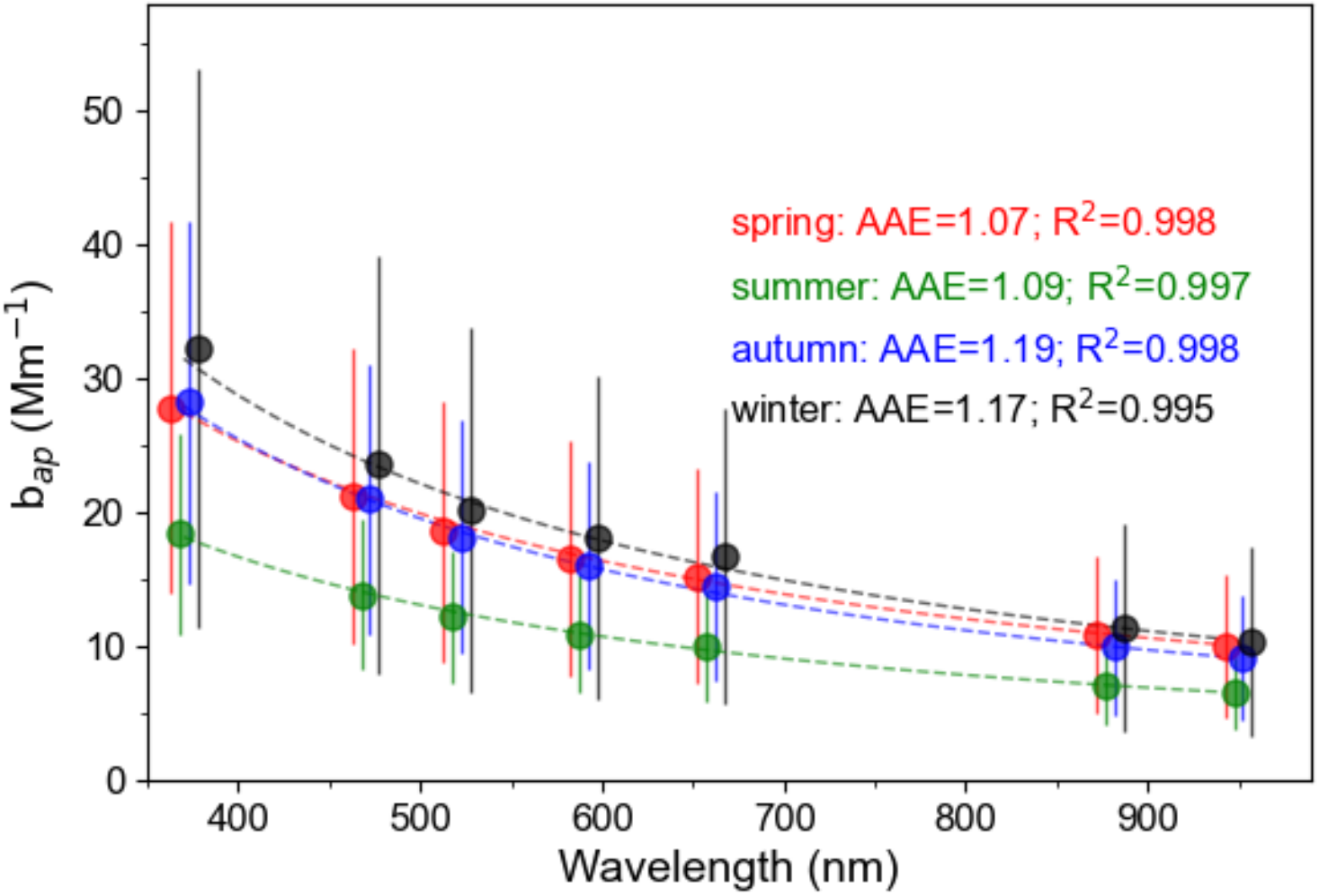
spring: AAE=1.07; R2=0.998
summer: AAE=1.09; R2=0.997
autumn: AAE=1.19; R2=0.998
winter: AAE=1.17; R2=0.995
bap (Mm−1)
Wavelength (nm)
0
10
20
30
40
50
400
500
600
700
800
900

Fig.5

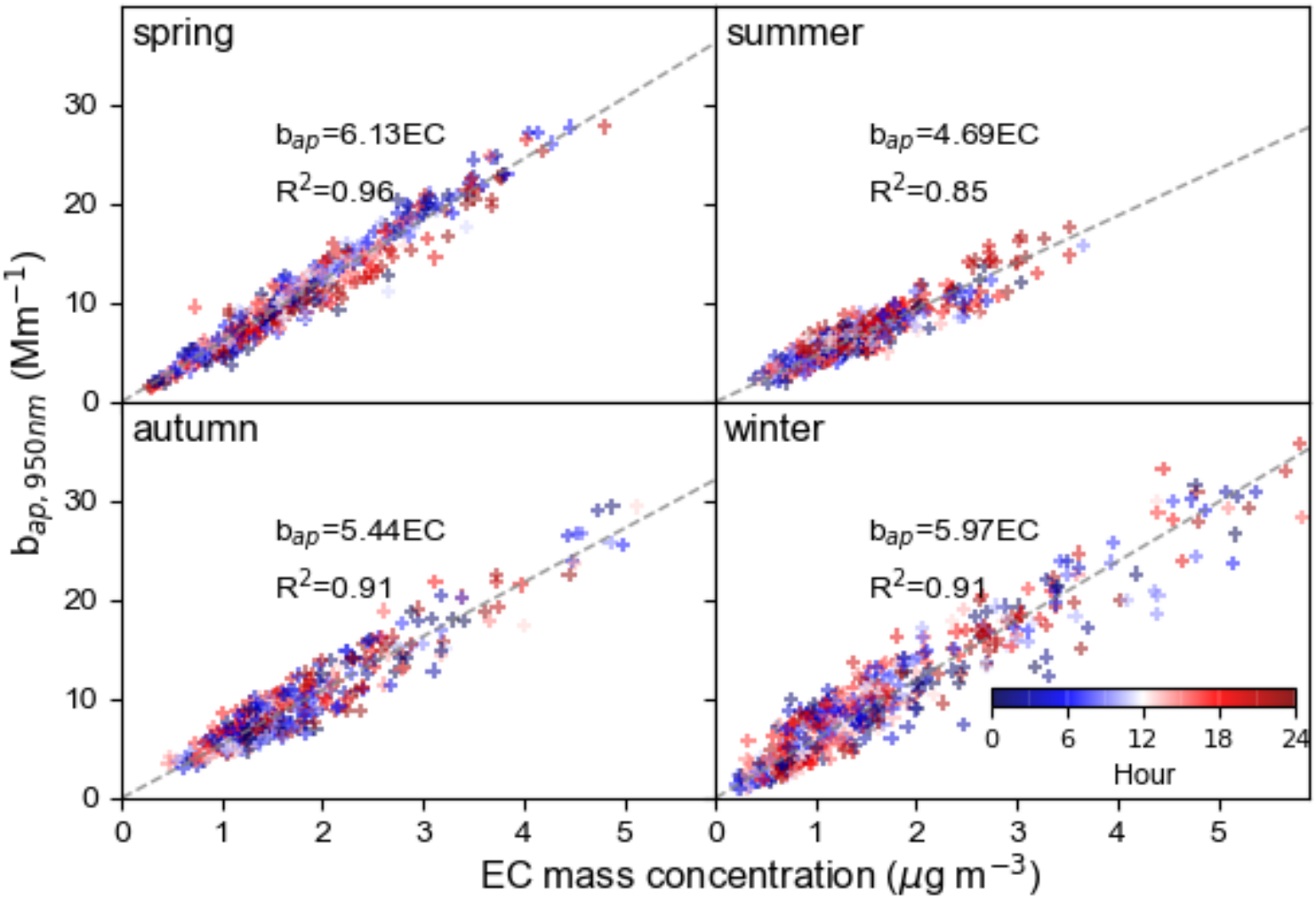
spring
summer
autumn
winter
b_{ap}=6.13EC
R^2=0.96
b_{ap}=4.69EC
R^2=0.85
b_{ap}=5.44EC
R^2=0.91
b_{ap}=5.97EC
R^2=0.91
$b_{ap,950nm}$ (Mm^{-1})
EC mass concentration (μg m^{-3})
0
6
12
18
24
Hour

Fig.6

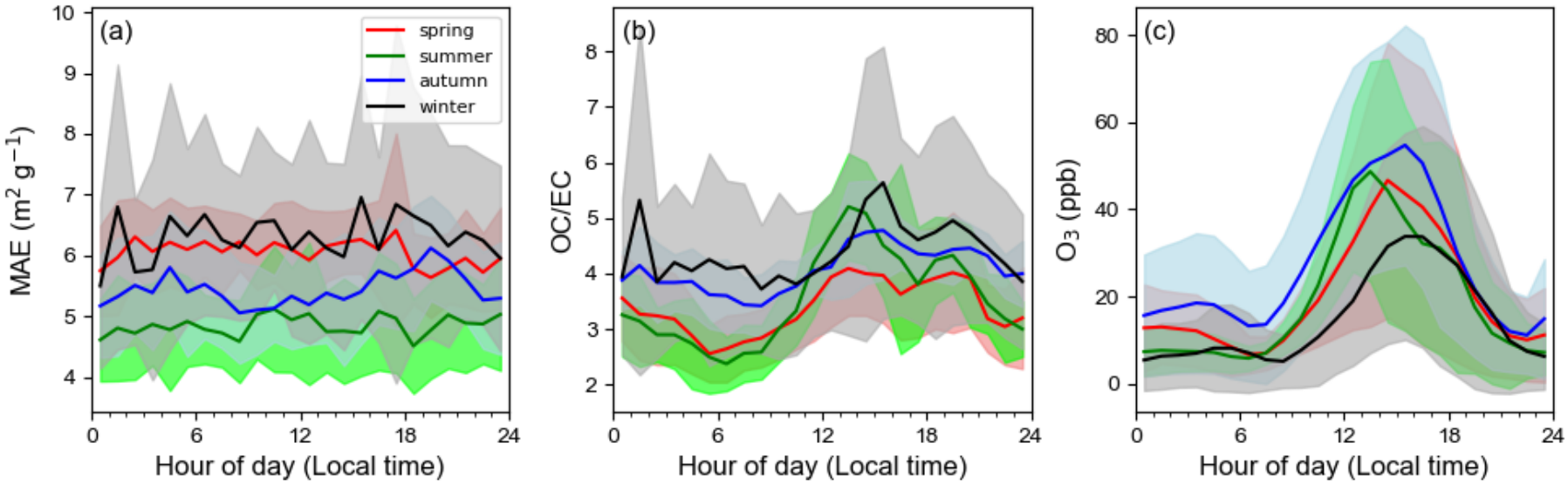
(a)
spring
summer
autumn
winter
MAE (m^2 g^{-1})
Hour of day (Local time)
(b)
OC/EC
Hour of day (Local time)
(c)
O_3 (ppb)
Hour of day (Local time)

Fig.7

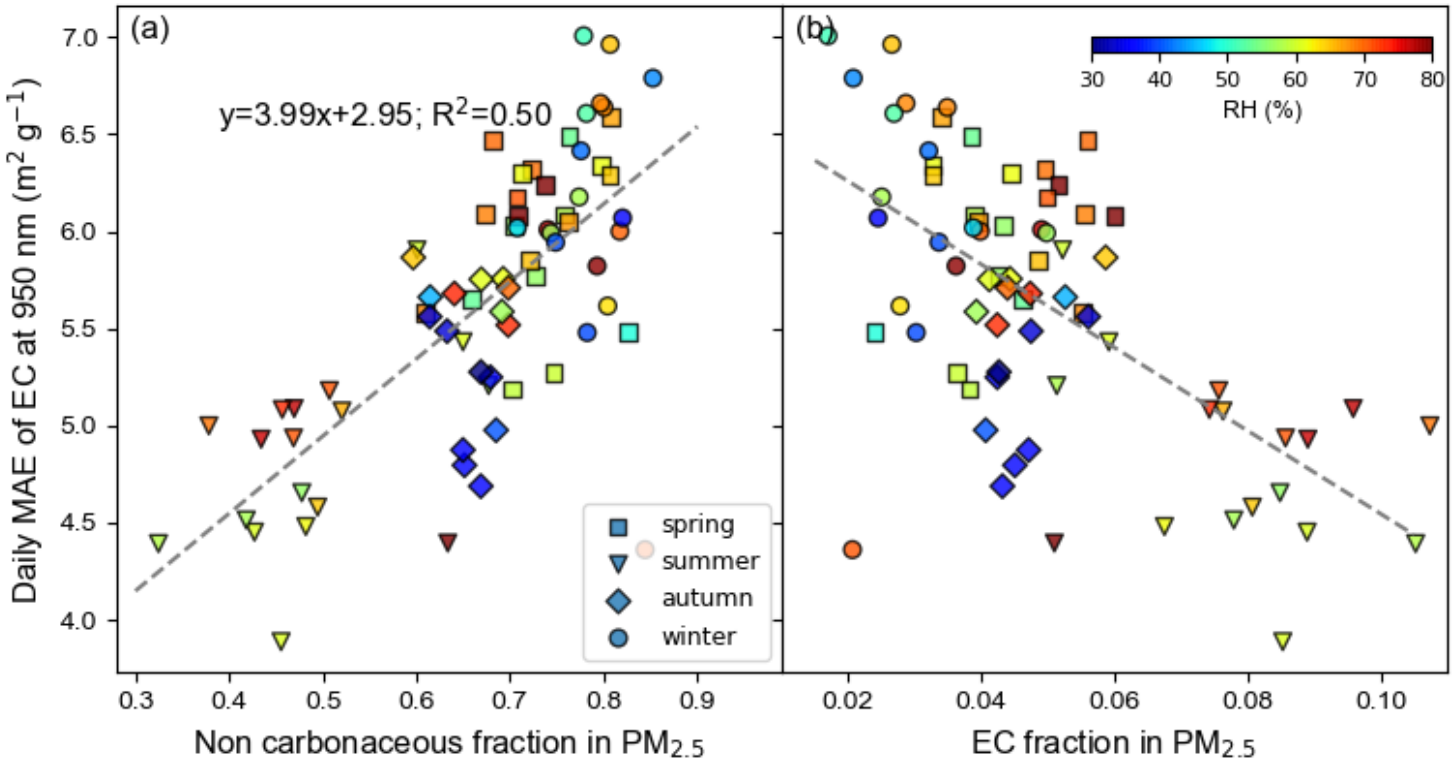
(a)
y=3.99x+2.95; R2=0.50
Daily MAE of EC at 950 nm (m2 g−1)
Non carbonaceous fraction in PM2.5
spring
summer
autumn
winter
(b)
RH (%)
EC fraction in PM2.5

Fig.8

Supplemental files for

Seasonal variations of mass absorption efficiency of elemental carbon in $PM_{2.5}$ in urban Guangzhou of south China

by Chenglei Pei et al.

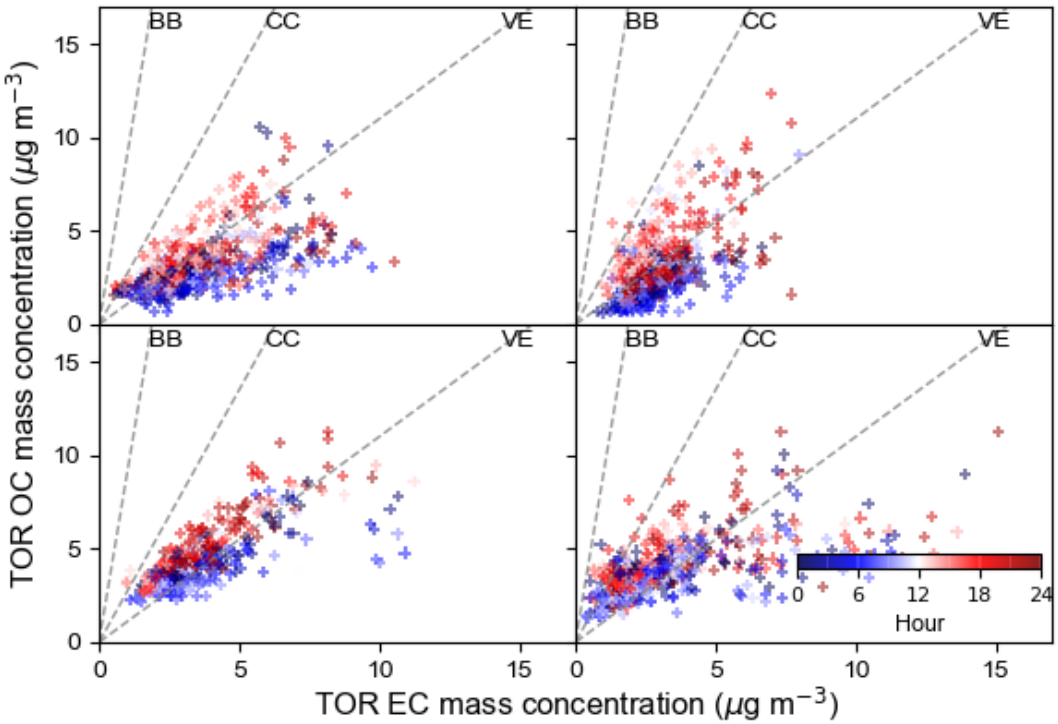

Fig. S1 Scatter plots of hourly mass concentration of OC versus EC under the IMPROVE-TOR protocol in four seasons. The TOR EC mass concentrations were calculated from the measured EC mass concentrations using the NIOSH-TOT protocol by considering a conversion factor of 2.2 proposed by Wu et al. (2016). The TOR OC mass concentrations were then calculated by subtracting the TOR EC mass concentrations from the total carbon mass concentrations, which are the sum of measured OC and EC concentrations. Dashed lines represent the typical TOR OC/EC mass ratios for biomass burning (BB, 9), coal combustion (CC, 2.7) and vehicle exhaust (VE, 1.1), respectively, proposed by Waston et al. (2001).

References

Wu, C, Huang, X H H, Ng, W M, Griffith, S M, Yu, J Z, 2016a. Inter-comparison of NIOSH and

IMPROVE protocols for OC and EC determination: implications for inter-protocol data conversion. Atmos. Meas. Tech. 9:4547-4560.

Watson, J G, Chow, J C, Houck, J E, 2001. PM2.5 chemical source profiles for vehicle exhaust, vegetative burning, geological material, and coal burning in Northwestern Colorado during 1995. Chemosphere 43:1141-1151.